

An Asymptotically Reduced Model of Langmuir Turbulence

GREGORY P. CHINI[†]

W113 Kingsbury Hall, Department of Mechanical Engineering, University of New Hampshire
Durham, NH 03824

Phone: (603) 862-2633 Fax: (603) 862-1865 Email: greg.chini@unh.edu

KEITH JULIEN

321 ECOT, Department of Applied Mathematics, University of Colorado–Boulder
Boulder, CO 80309-0526

Phone: (303) 492-5753 Fax: (303) 492-4066 Email: Keith.Julien@colorado.edu

EDGAR KNOBLOCH

457 Birge, Department of Physics, University of California–Berkeley, Berkeley, CA 94720-7300

Phone: (510) 642-3395 Fax: (510) 643-8497 Email: knobloch@tardis.berkeley.edu

(January 31st, 2008)

An asymptotically exact reduced model describing Langmuir turbulence in the strong surface wave forcing limit is constructed. Linear and secondary stability analyses suggest that the reduced dynamics exhibit the dominant instability modes arising in highly supercritical Langmuir circulation. The model appears to capture the essential physics of strongly anisotropic Langmuir turbulence, and may be more amenable to analysis than the three-dimensional Craik-Leibovich equations from which the reduced equation set is derived.

Keywords: Convection; Langmuir Circulation; Multiscale Asymptotic Analysis; Reduced Equations; Ocean Mixed Layer; Streamwise Vortices.

[†]Corresponding author. Email: greg.chini@unh.edu

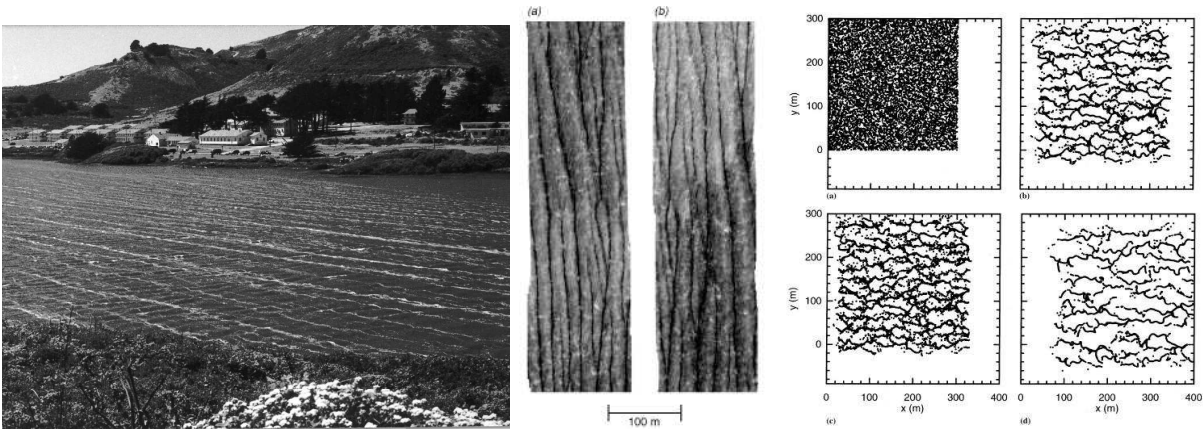


Figure 1. Images of Langmuir circulation windrows: (a) a photograph of Rodeo Lagoon in CA (Szeri 1996), (b) an infrared image of the surface of Tampa Bay (courtesy of G. Marmorino, NRL, D.C.), and (c) the evolution of surface tracers in a LES of Langmuir turbulence (McWilliams et al. 1997).

1 Introduction

Langmuir circulation (LC) is a wind and surface-wave driven convective flow that commonly occurs in the upper layers of lakes, rivers and oceans (Leibovich 1983, Thorpe 2004). When the winds exceed a few meters per second, LC exhibits a range of length and times scales, from centimetres to hundreds of meters and seconds to hours. The emergence of a broad spectrum of scales prompted McWilliams et al. (1997) to dub this phenomenon “Langmuir turbulence,” both to emphasize that LC is properly viewed as part of the upper ocean turbulence and to distinguish it from wall-bounded shear flow turbulence. Even under uncontrolled, strongly supercritical environmental conditions, however, LC is dominated by energetic counter-rotating streamwise vortical structures. These structures are elongated in the wind direction when the wind-driven shear and surface-wave Stokes drift are themselves aligned with the wind or to the right of the wind direction when Coriolis effects are significant. In view of this evident anisotropy, the aim of the present study is to derive a coarse-grained, quasi-three-dimensional description of Langmuir turbulence.

Figure 1 shows several illustrations of the hallmark surface signature of LC: a series of roughly parallel, wind-aligned streaks. These “windrows” are evident visually (figure 1(a)), in infrared and acoustic imagery (figure 1(b)), and in full three-dimensional (3D) direct numerical and large-eddy simulations (DNS and LES, respectively – figure 1(c)). To date, the vast majority of numerical simulations of LC have employed the Craik–Leibovich (CL) equations, a surface-wave filtered version of the Navier–Stokes (NS) equations; see Craik and Leibovich (1976), Craik (1977) and Leibovich (1977). The CL equations are formally identical to the instantaneous NS equations apart from the occurrence of a vortex-force term given by the cross product of the Stokes (or Lagrangian mass) drift velocity, associated with the high-frequency waves, and the filtered vorticity vector in the water column. The CL vortex force captures the rectified effects of the filtered waves on the time-averaged dynamics. Numerous investigators, inspired by the appearance of the locally parallel windrows, have carried out theoretical studies and numerical simulations of the 2D (generally downwind invariant) CL equations; see e.g. Leibovich (1985), Leibovich et al. (1989), Cox et al. (1992*a*), Cox et al. (1992*b*), Cox and Leibovich (1994), Chini and Leibovich (2003), Chini and Leibovich (2005), Li and Garrett (1993), Gnanadesikan and Weller (1995) and Li and Garrett (1997). With the exception of the secondary stability analysis of Tandon and Leibovich (1995), however, investigations of the stability of 2D roll solutions of the CL equations to 3D disturbances have been restricted to weakly supercritical forcing conditions, where weakly nonlinear or small wavenumber (i.e. large cell aspect-ratio) approximations can be utilized (Cox and Leibovich 1997, Bhaskaran and Leibovich 2002).

In this investigation, we develop a strongly nonlinear quasi-3D approach that relaxes the assumptions of strict downwind invariance and weak supercriticality yet exploits the slow downwind variability of the appropriately coarse-grained flow. Specifically, we obtain a reduced description of Langmuir turbulence

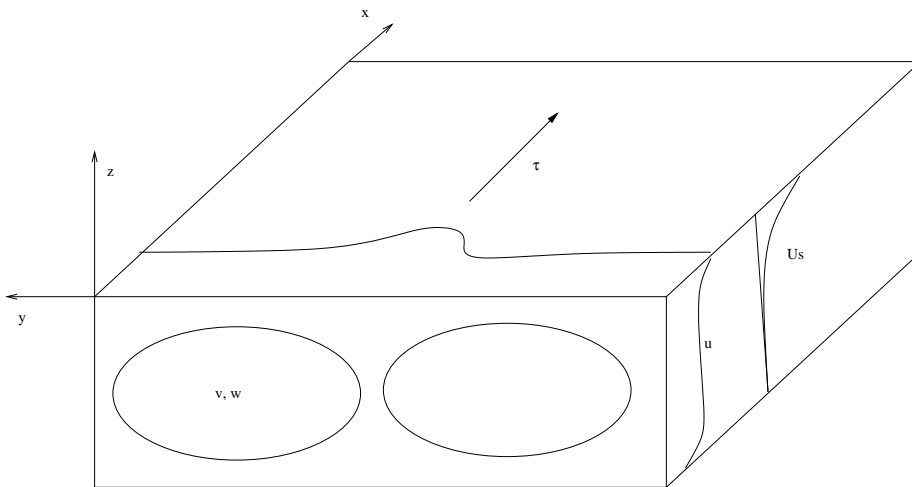


Figure 2. Schematic of Langmuir circulation in a constant-depth unstratified layer. τ is the magnitude of the applied wind stress; u , v and w are the x -, y - and z -velocity components; and U_s is the depth-varying Stokes drift velocity associated with the filtered surface waves.

that is formally valid in the strong CL vortex-force limit. To this end, we note that the secondary stability results of Tandon and Leibovich (1995) indicate that as a certain parameter related to the strength of the wave forcing is increased, so, too, is the downwind (i.e. along-roll) wavelength of the dominant 3D instability mode. This result points to a tendency for the highly nonlinear, locally averaged flow to be modulated in the downwind direction over a length scale that is large compared to the windrow spacing. Our analysis is similar in spirit, if not in detail, to that by Julien, Knobloch and co-workers for rapidly-rotating Rayleigh–Bénard convection (Julien et al. 1998, Sprague et al. 2006, Julien et al. 2006). These authors were able to obtain a reduced description of turbulent thermal convection by exploiting the reduction in mode coupling parallel to the rotation vector induced by the rapid rotation. As demonstrated in the next section, the relevant constraint on the turbulence in the LC context is provided by strong wave (i.e. vortex) forcing rather than by rapid system rotation.

The outline of the paper is as follows. In § 2, the CL equations are recounted and the merits of investigating the limit of strong surface-wave forcing are discussed. Next, the decomposition of the limiting dynamics into a fast and slow set is described in § 3, where a transient rapid distortion behaviour is identified. A reduced set of partial differential equations (PDEs) governing quasi-3D Langmuir turbulence is derived in § 4. In § 5, the physical processes captured by the reduced system are discussed. Results of linear and secondary (i.e. nonlinear) stability analyses of the reduced system are summarized in § 6, and concluding remarks are given in § 7.

2 Problem formulation

Using a coordinate system in which x is aligned with the wind, y is directed across the wind and z vertically upward (see figure 2), the non-dimensional CL equations in the absence of density stratification and background rotation (Coriolis effects) can be written as

$$\frac{D\mathbf{u}}{Dt} = -\nabla p + \frac{1}{La_t^2}(\mathbf{U}_s \times \boldsymbol{\omega}) + \frac{1}{R_*} \nabla^2 \mathbf{u}, \quad (1)$$

along with the incompressibility constraint

$$\nabla \cdot \mathbf{u} = 0. \quad (2)$$

In (1), $R_* \equiv u_* H / \nu_e$ is the Reynolds number based on the water friction velocity u_* , the depth of the convective (or mixed) layer H and the (eddy) viscosity ν_e arising from the CL wave filtering procedure. The turbulent Langmuir number $La_t \equiv (u_* / u_{s_0})^{1/2}$, where u_{s_0} is the surface Stokes drift velocity (McWilliams et al. 1997). The total (filtered) Eulerian velocity vector $\mathbf{u} = u\hat{i} + \mathbf{v}_\perp$, where $\mathbf{v}_\perp = v\hat{j} + w\hat{k}$ is the cross-wind velocity field, and the vorticity vector $\boldsymbol{\omega} = \nabla \times \mathbf{u}$. All lengths and velocity components have been non-dimensionalized isotropically using H and u_* , respectively. Time t has been scaled by H/u_* and the (CL modified) pressure p by ρu_*^2 , where ρ is the mean water density. Typically, the normalized Stokes drift profile is taken to be an exponentially decaying function of depth,

$$\mathbf{U}_s(z) = U_s(z)\hat{i} = \exp(2\beta z)\hat{i}, \quad (3)$$

although any monotonically-decaying profile will give rise to similar phenomenology. A representative value of the e-folding depth of the Stokes drift, $1/(2\beta)$, is $0.2H$.

Since the surface waves are filtered in the CL formulation, the (filtered) vertical velocity vanishes at the mean position of the sea surface, taken to be $z = 0$, and at the base of the layer ($z = -1$). As shown in figure 2, the wind stress and surface wave Stokes drift are assumed to be aligned in the x direction. The wind applies a traction that in the CL formulation is also applied at the mean position of the sea surface. Thus, at $z = 0$,

$$\partial_z u = R_*, \quad \partial_z v = 0, \quad w = 0, \quad (4)$$

and at $z = -1$,

$$\partial_z u = R_*, \quad \partial_z v = 0, \quad w = 0 \quad (5)$$

or

$$u = 0, \quad v = 0, \quad w = 0, \quad (6)$$

depending upon whether the bottom boundary is a surface representing the base of the mixed layer or a physical, no-slip boundary, respectively. All flowfields are taken to be periodic in the x and y directions.

As noted in § 1, the central idea in the derivation of a weakly 3D description of Langmuir turbulence is to exploit the limit in which the CL vortex force dominates the flow physics. This limit corresponds to increasing the surface-wave Stokes drift relative to the wind-driven shear. Although both u_{s_0} and u_* are expected to increase together for locally-generated wind waves, La_t in the open ocean typically is $O(0.1)$. This motivates us to consider the limiting process in which $La_t \rightarrow 0$ while R_* either remains fixed or, more generally, may tend to infinity (see § 4). LES by Skillingstad and Denbo (1995), McWilliams et al. (1997) and Tejada-Martinez and Grosch (2007) have demonstrated that ordinary shear flow turbulence is recovered in the opposite limit $La_t \rightarrow \infty$ with R_* sufficiently large. Indeed, La_t may be seen to measure the competition between shear and vortex-force induced instability of the wind-driven currents. Although streamwise vortices arise in wall-bounded turbulent shear flows, these structures differ (e.g. in terms of their energetics, root-mean-square fluctuation intensities and coherence in the mean flow direction) from those characterizing LC. Immediate insight into the origin of the anisotropy in Langmuir turbulence may be gained by considering the $La_t \rightarrow 0$ limit of (1), (naively) holding other variables fixed: it is readily concluded that the vorticity vector must be parallel to the Stokes drift, i.e. to the wind direction. By formally exploiting the small La_t limit using multiple scale asymptotics, we are able to relax the assumption of strict downwind invariance, and thereby identify the dominant 3D physical processes in anisotropic Langmuir turbulence.

3 Fast linear dynamics and the spatially-2D slow manifold

In the small La_t (i.e. large CL vortex-force) limit, the leading-order dynamics may be decomposed into fast and slow components. First, we write (1) in component form:

$$\partial_t u + u\partial_x u + v\partial_y u + w\partial_z u = -\partial_x p + R_*^{-1} [\partial_x^2 + \partial_y^2 + \partial_z^2] u, \quad (7)$$

$$\partial_t v + u\partial_x v + v\partial_y v + w\partial_z v = -\partial_y p + La_t^{-2} U_s (\partial_y u - \partial_x v) + R_*^{-1} [\partial_x^2 + \partial_y^2 + \partial_z^2] v, \quad (8)$$

$$\partial_t w + u\partial_x w + v\partial_y w + w\partial_z w = -\partial_z p + La_t^{-2} U_s (\partial_z u - \partial_x w) + R_*^{-1} [\partial_x^2 + \partial_y^2 + \partial_z^2] w. \quad (9)$$

Next, to capture a fast linear response, we rescale time $t = La_t^2 \tau$ and pressure $p = La_t^{-2} \mathcal{P}$. As $La_t \rightarrow 0$, equations (7)–(9) simplify, at leading order, to

$$\partial_\tau u = -\partial_x \mathcal{P}, \quad (10)$$

$$\partial_\tau v = -\partial_y \mathcal{P} + U_s (\partial_y u - \partial_x v), \quad (11)$$

$$\partial_\tau w = -\partial_z \mathcal{P} + U_s (\partial_z u - \partial_x w). \quad (12)$$

Employing standard manipulations and using the incompressibility constraint, (10)–(12) can be recast in a vertical-vorticity–vertical-velocity formulation,

$$\partial_\tau \omega_z + U_s \partial_x \omega_z = 0, \quad (13)$$

$$\partial_\tau (\nabla^2 w) + U_s \partial_x (\nabla^2 w) = U'_s(z) \partial_y \omega_z, \quad (14)$$

where the vertical vorticity $\omega_z = \partial_x v - \partial_y u$ and the prime denotes ordinary differentiation. The solution to this initial value problem can be expressed as:

$$\omega_z(x, y, z, \tau) = \omega_{z_0}(x - U_s(z)\tau, y, z), \quad (15)$$

$$\nabla^2 w(x, y, z, \tau) = [U'_s(z) \partial_y \omega_{z_0}(x - U_s(z)\tau, y, z)] \tau + \nabla^2 w_0(x - U_s(z)\tau, y, z), \quad (16)$$

where $\omega_{z_0}(x, y, z)$ and $w_0(x, y, z)$ are the initial vertical-vorticity and vertical-velocity components, respectively. This solution indicates that the vertical vorticity is merely passively advected over the fast time scale τ by the differential Stokes drift: at a given depth z , in a local reference frame translating in the x -direction with speed $U_s(z)$, the vertical vorticity is τ -independent. In this frame, (16) shows that the vertical velocity grows linearly with τ .

The physics of this fast-time, linear response in the strong vortex-force limit can be more clearly understood by restricting attention to downwind invariant dynamics. Indeed, the linear stability analyses of Leibovich and Tandon (1993) and Cox (1997) demonstrate that in a homogeneous fluid layer the fastest growing instabilities to a horizontally-uniform wind-driven shear flow $U_B(z) = z+1$ (with associated pressure $P_B(z)$ satisfying $dP_B/dz = U_s dU_B/dz$) take the form of x -invariant roll vortices aligned with the wind. Thus, it is instructive to consider the fast-time response of $U_B(z)$ to 2D downwind velocity perturbations $\tilde{u}(y, z, \tau)$. Setting x -derivatives to zero, (10)–(12) become:

$$\partial_\tau \tilde{u} = 0, \quad (17)$$

$$\partial_\tau \tilde{v} = -\partial_y \tilde{\mathcal{P}} + U_s \partial_y \tilde{u}, \quad (18)$$

$$\partial_\tau \tilde{w} = -\partial_z \tilde{\mathcal{P}} + U_s \partial_z \tilde{u}, \quad (19)$$

where tildes denote perturbation variables. Subtracting the z -derivative of (18) from the y -derivative of

(19) yields a fast time evolution equation for the downwind vorticity $\tilde{\Omega}(y, z, \tau)$,

$$\partial_\tau \tilde{\Omega} = -U'_s(z) \partial_y \tilde{u}. \quad (20)$$

Equation (17) implies that the downwind velocity perturbation is independent of the fast time variable, i.e. $\tilde{u}(y, z, \tau) \equiv \tilde{U}(y, z)$. Using this result, the solution to (20) is

$$\tilde{\Omega}(y, z, \tau) = - \left[U'_s(z) \partial_y \tilde{U}(y, z) \right] \tau + \tilde{\Omega}_0(y, z), \quad (21)$$

where $\tilde{U}(y, z)$ and $\tilde{\Omega}_0(y, z)$ are the initial downwind velocity and vorticity perturbations, respectively. Thus, the downwind vorticity and, hence, \tilde{v} and \tilde{w} grow linearly in the fast time variable.

This rapid-distortion solution, in which an initial vertical vorticity perturbation is tilted in the wind direction by the strongly “sheared” Stokes drift (note that $U_s(z)$, the Lagrangian mass drift velocity associated with *irrotational* surface waves, is *not* a shear flow), must lose validity when the x vorticity created by this process becomes large enough to feed back upon the downwind velocity component. In § 4, we identify a new dominant balance in which the secular growth of the downwind vorticity is arrested and the evolution occurs on a slow manifold. Suppressing τ -derivatives in (10)–(12) reveals the 2D spatial character of this manifold, for then

$$\nabla \mathcal{P} = \mathbf{U}_s \times \boldsymbol{\Omega}, \quad (22)$$

where $\boldsymbol{\Omega} = \nabla \times \mathbf{U}$ is the leading-order vorticity vector and $\mathbf{U} = U\hat{i} + V\hat{j} + W\hat{k}$ is the leading order velocity vector on the slow manifold. The x -component of (22), which itself is loosely analogous to the geostrophic balance arising at small scales in rapidly rotating convection, gives $\partial_x \mathcal{P} = 0$. The absence of a leading-order fine-scale x -pressure variation (in conjunction with the incompressibility constraint) clearly indicates that the slow dynamics are 2D. Indeed, taking the curl of (22) yields

$$\mathbf{U}_s \cdot \nabla \boldsymbol{\Omega} = \boldsymbol{\Omega} \cdot \nabla \mathbf{U}_s, \quad (23)$$

and expressing the vorticity vector $\boldsymbol{\Omega} = \Omega_x \hat{i} + \Omega_y \hat{j} + \Omega_z \hat{k}$, (23) in component form becomes

$$U_s \partial_x \Omega_x = \Omega_z U'_s(z), \quad (24)$$

$$U_s \partial_x \Omega_y = 0, \quad (25)$$

$$U_s \partial_x \Omega_z = 0. \quad (26)$$

Since $\partial_x \mathcal{P} = \partial_x \Omega_y = \partial_x \Omega_z = 0$, the leading-order dynamics on the slow manifold are (fast-) x -invariant, and the leading-order incompressibility constraint reduces to

$$\partial_y \mathcal{V} + \partial_z \mathcal{W} = 0, \quad (27)$$

implying that a streamfunction can be introduced to describe the flow in the y - z plane.

4 Fully nonlinear quasi-3D dynamics

The analysis in § 3 suggests that cross-wind (generally cellular) velocity fluctuations can rapidly attain large magnitudes when $La_t \ll 1$, while the magnitude of downwind velocity fluctuations remains fixed. The secular growth of the downwind vorticity equilibrates on a longer time scale through a nonlinear feedback mechanism in which the cross-wind velocity fluctuations are sufficiently intense to alter the downwind velocity distribution. This motivates rescaling the downwind and cross-wind velocity components in the *dimensional* CL equations anisotropically. Specifically, we scale the downwind velocity component with

$U_* \equiv u_* R_*$ and the cross-wind velocity components with $W_* \equiv (U_* u_{s_0})^{1/2}$. The former scaling ensures that the wind-stress forcing in the rescaled versions of (4) and (5) is $O(1)$, while the latter ensures that, even in the absence of downwind variability, the nonlinear advection terms in the cross-wind momentum equation are comparable to the CL vortex force, as required for equilibration of the rapid distortion transients. In addition, we scale time by H/W_* and pressure by ρW_*^2 to incorporate unsteadiness and cross-wind pressure gradients in the reduced dynamics.

Additional insight into the origin of these modified scalings may be gained from the following considerations. First, from (21), the dimensional magnitude of the crosswind velocity fluctuations will reach $O(W_*)$ after a time period $T_s = O(H/W_*)$, given an $O(u_* R_*)$ downwind velocity perturbation. It is over this time scale, which is long compared to the time scale $T_{RDT} = La_t^2(H/u_*)$ characterizing the rapid distortion transients, that the secular growth of the downwind vorticity is arrested and a new dynamical balance is possible. Moreover, the modified scalings are identical to those typically used to non-dimensionalize the strictly downwind invariant, i.e. 2D, CL equations (Craik and Leibovich 1976, Leibovich 1983, Li and Garrett 1993). In fact, with this set of scalings, the dynamics of the 2D problem (for a given domain size) are then governed by a *single* non-dimensional parameter, the so-called *laminar* Langmuir number $La \equiv La_t R_*^{-3/2}$, which replaces the two parameters needed to describe the fully 3D dynamics of Langmuir turbulence. As demonstrated in § 3, the limiting dynamics on the slow manifold are only weakly three-dimensional. To obtain a reduced formulation, we essentially perturb about a downwind invariant flow; thus, it is sensible to rescale variables in (1) to accord with the scalings appropriate for the strictly 2D problem.

The rescaled CL equations, in momentum form, can be written:

$$\partial_T u + R_*^{1/2} La_t u \partial_x u + (\mathbf{v}_\perp \cdot \nabla_\perp) u = -(R_*^{1/2} La_t)^{-1} \partial_x P + R_*^{-3/2} La_t [\partial_x^2 + \nabla_\perp^2] u, \quad (28)$$

$$\begin{aligned} \partial_T \mathbf{v}_\perp + R_*^{1/2} La_t u \partial_x \mathbf{v}_\perp + (\mathbf{v}_\perp \cdot \nabla_\perp) \mathbf{v}_\perp = & -\nabla_\perp P + U_s \left[\nabla_\perp u - (R_*^{1/2} La_t)^{-1} \partial_x \mathbf{v}_\perp \right] \\ & + R_*^{-3/2} La_t [\partial_x^2 + \nabla_\perp^2] \mathbf{v}_\perp, \end{aligned} \quad (29)$$

$$R_*^{1/2} La_t \partial_x u + \nabla_\perp \cdot \mathbf{v}_\perp = 0. \quad (30)$$

Although we have introduced new notation for the rescaled pressure (P) and time (T), note that we have not done so for the rescaled velocity vector $\mathbf{u} = u\hat{i} + \mathbf{v}_\perp$ (where $\mathbf{v}_\perp = v\hat{j} + w\hat{k}$). Formally, the boundary conditions in (4) and (5) remain unchanged, except that the flux conditions become $\partial_z u = 1$ at $z=0$ and $z=-1$. Defining $\varepsilon \equiv R_*^{1/2} La_t$, we formally investigate the limit in which $\varepsilon \rightarrow 0$, i.e. $La_t \rightarrow 0$ with $R_* = La_t^{-2\alpha/(1-\alpha)}$ for $0 \leq \alpha < 1/2$ (cf. §2). Note that this corresponds to $1 \leq R_* < La_t^{-2}$, which implies that our reduced formulation will be valid over a fairly broad parameter regime, encompassing R_* fixed and $O(1)$ at one extreme and R_* an asymptotically large parameter at the other. To capture weak downwind variability, we introduce a slow x -scale $X \equiv \varepsilon x$ so that

$$\partial_x(\cdot) \rightarrow \partial_x(\cdot) + \varepsilon \partial_X(\cdot),$$

and we expand all field variables as follows:

$$u(x, y, z, T) = u_0(x, X, y, z, T) + \varepsilon u_1(x, X, y, z, T) + \dots \quad (31)$$

$$\mathbf{v}_\perp(x, y, z, T) = \mathbf{v}_{0\perp}(x, X, y, z, T) + \varepsilon \mathbf{v}_{1\perp}(x, X, y, z, T) + \dots \quad (32)$$

$$P(x, y, z, T) = P_0(x, X, y, z, T) + \varepsilon P_1(x, X, y, z, T) + \dots \quad (33)$$

Substituting into (28)–(30), we find that $\partial_x P_0 = \partial_x v_0 = \partial_x w_0 = 0$ and $\nabla_\perp \cdot \mathbf{v}_{0\perp} = 0$, confirming that the leading-order flow is independent of the fast x coordinate. At $O(1)$, (28) becomes:

$$\partial_T u_0 + (\mathbf{v}_{0\perp} \cdot \nabla_\perp) u_0 = -\partial_x P_1 - \partial_X P_0 + La \nabla_\perp^2 u_0, \quad (34)$$

where the cross-wind diffusion terms, formally $O(La_t R_*^{-3/2})$, have been retained to allow for the existence of thin viscous boundary and internal layers in which their influence cannot be neglected. We decompose all (fast) x -varying fields into a fast- x average plus a fluctuation, e.g.

$$u_0(x, X, y, z, T) \equiv \bar{u}_0(X, y, z, T) + u'_0(x, X, y, z, T),$$

where the bar is used to denote the average and the prime the fluctuation. Averaging (34) in x , and exploiting the leading-order x -invariance of the pressure and cross-wind velocity components, we obtain an evolution equation for $\bar{u}_0(X, y, z, T)$:

$$\partial_T \bar{u}_0 + (\mathbf{v}_{0\perp} \cdot \nabla_{\perp}) \bar{u}_0 = -\partial_X P_0 + La \nabla_{\perp}^2 \bar{u}_0. \quad (35)$$

Similarly, the $O(1)$ version of (29) is given by

$$\partial_T \mathbf{v}_{0\perp} + (\mathbf{v}_{0\perp} \cdot \nabla_{\perp}) \mathbf{v}_{0\perp} = -\nabla_{\perp} P_0 + U_s \nabla_{\perp} u_0 - U_s \partial_x \mathbf{v}_{1\perp} - U_s \partial_X \mathbf{v}_{0\perp} + La \nabla_{\perp}^2 \mathbf{v}_{0\perp}. \quad (36)$$

The formally small diffusion terms have again been retained in anticipation of the existence of thin viscous layers at small La . Averaging over the fast x -coordinate gives

$$\partial_T \mathbf{v}_{0\perp} + (\mathbf{v}_{0\perp} \cdot \nabla_{\perp}) \mathbf{v}_{0\perp} = -\nabla_{\perp} P_0 + U_s (\nabla_{\perp} \bar{u}_0 - \partial_X \mathbf{v}_{0\perp}) + La \nabla_{\perp}^2 \mathbf{v}_{0\perp}. \quad (37)$$

The reduced system is closed by invoking the $O(1)$ continuity equation,

$$\nabla_{\perp} \cdot \mathbf{v}_{0\perp} = 0, \quad (38)$$

from which a Poisson equation for $P_0(X, y, z, T)$ can be derived, *viz.*

$$\nabla_{\perp}^2 P_0 = -\nabla_{\perp} \cdot \left((\mathbf{v}_{0\perp} \cdot \nabla_{\perp}) \mathbf{v}_{0\perp} \right) + \nabla_{\perp} \cdot \left(U_s(z) \nabla_{\perp} \bar{u}_0 \right) - U'_s(z) \partial_X w_0. \quad (39)$$

We conclude this section by noting that the $O(1)$ stress boundary condition at the top and bottom of the convection zone, averaged over the fast x variable, is given by

$$\partial_z \bar{u}_0|_{z=0, -1} = 1. \quad (40)$$

5 Synopsis of reduced system in streamfunction/vorticity form

Equations (35), (37) and either (38) or (39) constitute a closed system governing quasi-3D Langmuir turbulence in the strong CL vortex-force limit. Using (38), a streamfunction ψ can be introduced. The reduced system can then be expressed more conveniently in a streamfunction/vorticity formulation closely mimicking that frequently used for the strictly 2D CL equations. Defining $\bar{u}_0 \equiv U(X, y, z, T)$, $v_0 \equiv V(X, y, z, T)$, $w_0 \equiv W(X, y, z, T)$ and $P_0 \equiv \Pi(X, y, z, T)$, and introducing the leading-order substantial derivative operator

$$\begin{aligned} D_t^{\perp}(\cdot) &\equiv \partial_T(\cdot) + (\mathbf{V}_{\perp} \cdot \nabla_{\perp})(\cdot), \\ &\equiv \partial_T(\cdot) + J[(\cdot), \psi], \end{aligned}$$

where $\mathbf{V}_{\perp} \equiv \mathbf{v}_{0\perp} \equiv \nabla \times \psi \hat{i}$ and $J[(\cdot), \psi] = \partial_z \psi \partial_y(\cdot) - \partial_y \psi \partial_z(\cdot)$, the reduced dynamics are governed by:

$$D_t^{\perp} U = -\partial_X \Pi + La \nabla_{\perp}^2 U, \quad (41)$$

$$D_t^{\perp} \Omega + U_s(z) \partial_X \Omega = U'_s(z) (\partial_X V - \partial_y U) + La \nabla_{\perp}^2 \Omega, \quad (42)$$

$$\nabla_{\perp}^2 \Pi = 2J[\partial_y \psi, \partial_z \psi] + \nabla_{\perp} \cdot \left(U_s(z) \nabla_{\perp} U \right) + U_s'(z) \partial_X (\partial_y \psi), \quad (43)$$

$$\nabla_{\perp}^2 \psi = -\Omega. \quad (44)$$

Equation (42) for the leading order downwind vorticity Ω is obtained by taking the x -component of the perpendicular curl of the cross-wind momentum equation (37). This system is supplemented by the leading-order (fast x -averaged) boundary conditions. At $z = 0$,

$$\partial_z U = 1, \quad \Omega = 0, \quad \psi = 0, \quad (45)$$

and at $z = -1$,

$$\partial_z U = 1, \quad \Omega = 0, \quad \psi = 0, \quad (46)$$

or

$$U = 0, \quad V = 0, \quad W = 0, \quad (47)$$

again depending upon whether stress-free or no-slip bottom boundary conditions are deemed more appropriate.

Although, formally, $La \equiv La_t R_*^{-3/2}$ is a small parameter, the asymptotic order of the diffusion terms retained in (41) and (42) increases in thin viscous layers that are generated at small La . Indeed, to neglect these terms would be a singular perturbation of the equations. An analogous situation arises in the derivation of the quasi-geostrophic equations, in which formally small horizontal diffusive terms are retained; see e.g. Pedlosky (1987). At the upper and lower boundaries of the domain, for example, boundary layers must arise to satisfy the imposed downwind traction condition. For vertical diffusion to balance advection in (41) and (42), the vertical thickness of these layers must be $O(La^{1/2})$, i.e. $Z \equiv La^{-1/2} z$, where $Z = O(1)$ is a scaled boundary layer vertical coordinate. The constant stress condition in (45) implies that the *change* in U across the near-surface boundary layer is $O(La^{1/2})$, while $\psi = O(La^{1/2})$ and $\Omega = O(1)$ within this layer. Similar scalings apply within vertical interior layers – that is, within narrow up- and downwelling jets – with the roles of y and z interchanged. We emphasize that with these rescalings, the normal diffusion terms are of the same asymptotic order as the other terms in the reduced equations, i.e. the reduced equations (41)–(44) constitute a *consistent* asymptotic approximation the full dynamics. It also should be noted that these small La scalings are identical to those given in Chini (2007), where a complete asymptotic characterization of steady 2D LC in the strong-forcing/weak-diffusion limit is given. There it is shown that the vorticity boundary layers are passive (assuming stress-free boundary conditions on the cellular flow), implying that they need not be resolved in a numerical simulation, and the streamfunction remains smooth, suggesting that far fewer modes are required to resolve ψ than Ω or U .

The linear and secondary stability properties of (41)–(44) are investigated quantitatively in § 6. However, several important attributes of the reduced system are immediately apparent. First, for X -invariant flows, this system collapses to the 2D CL equations in streamfunction/vorticity form. In contrast to the strictly 2D problem, however, the reduced system retains certain 3D physical processes involving slow downwind modulation. Equation (41) indicates that the downwind momentum of the flow can be altered by downwind pressure variations. According to (42), the downwind vorticity is *differentially* advected by the Stokes drift (recall U_s is a function of z). More significantly, the full contribution to the vertical vorticity, which is tilted into the wind direction by the Stokes drift gradient, is retained. Finally, in the Poisson equation for the pressure (43), slow downwind variations of the vertical velocity give rise to an additional vortex force contribution. Relative to the 2D problem, these important physical processes have been captured by the reduced system; relative to the full 3D CL equations, the reduced dynamics *suppress* certain physics, most notably advection by U and stretching of Ω by downwind gradients of U . It is the absence of vortex stretching, in particular, that should make (41)–(44) more amenable to theoretical (e.g. upper-

bound) analysis and numerical investigation than is the full system, because of the implied control on the generation of very fine scales. In addition, the reduced system filters the rapid distortion transients and incorporates differential advection of Ω in the X direction by the specified Stokes drift velocity, a linear process.

6 Stability analysis

Although we defer discussion of the numerical solution of the reduced system to future work, we record here the results of linear and secondary stability analyses of (41)–(44) subject to boundary conditions (45) and (46). We describe only a subset of the results, since our purpose is simply to illustrate the key 2D and 3D instabilities supported by the reduced system. No attempt is made here to carry out an exhaustive investigation of parameter space.

6.1 Linear stability results

We linearize (41)–(44) about the wind-driven base state shear flow $U_B(z) = z + 1$ and associated base state pressure distribution $d\Pi_B(z)/dz = U_s(z)$. For simplicity, we set $U_s(z) = z + 1$, as previous investigations have shown that LC stability characteristics are not qualitatively changed for more realistic, exponentially decaying Stokes drift profiles. Thus, we decompose all fields into a base state (which may be zero) plus a perturbation,

$$U(X, y, z, T) = U_B(z) + u(X, y, z, T), \quad (48)$$

$$\psi(X, y, z, T) = \phi(X, y, z, T), \quad (49)$$

$$\Pi(X, y, z, T) = \Pi_B(Z) + p(X, y, z, T), \quad (50)$$

$$\Omega(X, y, z, T) = \omega(X, y, z, T), \quad (51)$$

substitute into the reduced system (41)–(44) and boundary conditions (45)–(46), and linearize about the base state. Using the vertical component of the reduced equations in momentum form and these boundary conditions, it can be shown that $\partial_z \Pi = U_s$ along $z = 0$ and $z = -1$ and, hence, that the normal derivative of the perturbation pressure vanishes there. Thus, the perturbations satisfy

$$\partial_T u - \partial_y \phi = -\partial_x p + La \nabla_{\perp}^2 u, \quad (52)$$

$$\partial_T \omega + (z + 1) \partial_x \omega = \partial_x (\partial_z \phi) - \partial_y u + La \nabla_{\perp}^2 \omega, \quad (53)$$

$$\nabla_{\perp}^2 \phi = -\omega, \quad (54)$$

$$\nabla_{\perp}^2 p = \nabla_{\perp} \cdot [(z + 1) \nabla_{\perp} u] + \partial_x (\partial_y \phi), \quad (55)$$

subject to

$$\partial_z u = \omega = \phi = \partial_z p = 0 \quad (56)$$

along the upper and lower boundaries.

Since the flow is unbounded in the horizontal and the perturbation equations do not depend explicitly on the horizontal coordinates or time, we make a normal-mode *ansatz* for each perturbation variable. For example, we decompose the downwind velocity perturbation as follows:

$$u(X, y, z, T) = \hat{u}(z) e^{i(ky + lX)} e^{\sigma t} + \text{c.c.},$$

where k and l are the cross-wind and downwind wavenumbers of the disturbance mode, σ is the complex growth rate and c.c. denotes complex conjugate. Substituting into the perturbation equations and boundary

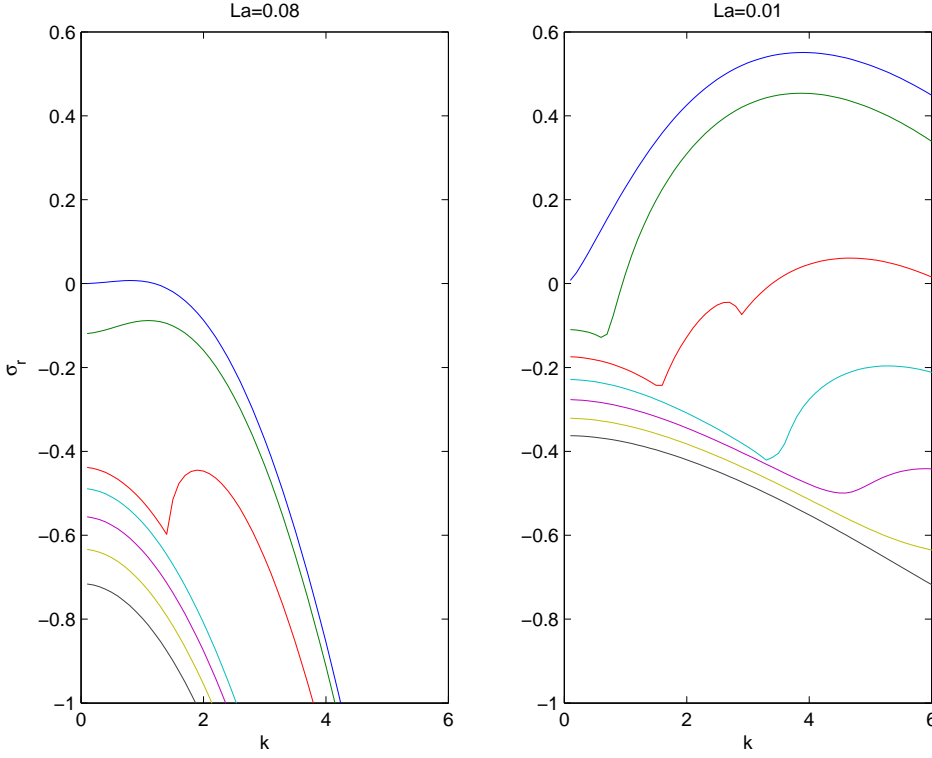


Figure 3. Linear stability results. The real part of the growth rate σ_r of the fastest growing mode is plotted versus cross-wind wavenumber k for various downwind wavenumbers l . In each plot, $l = 0$ for the uppermost curve, and $l = 1, 2, 3, 4, 5, 6$ increasing downward. (a) $La = 0.08$ (left). (b) $La = 0.01$ (right). 30 Chebyshev modes were used for all computations.

conditions and eliminating the vorticity from this set yields a linear ordinary differential eigenvalue problem for the growth rate:

$$La (D^2 - k^2) \hat{u} + ik\hat{\phi} - il\hat{p} = \sigma\hat{u}, \quad (57)$$

$$La (D^2 - k^2)^2 \hat{\phi} - il(z+1) (D^2 - k^2) \hat{\phi} + ik\hat{u} - ilD\hat{\phi} = \sigma (D^2 - k^2) \hat{\phi}, \quad (58)$$

$$(D^2 - k^2) \hat{p} - D\hat{u} + kl\hat{\phi} - (z+1) (D^2 - k^2) \hat{u} = 0, \quad (59)$$

where $D \equiv d/dz$. This system is solved subject to the following boundary conditions along $z=0$ and $z=-1$:

$$D\hat{u} = 0, \quad \hat{\phi} = 0, \quad D^2\hat{\phi} = 0. \quad (60)$$

We discretize the system (57)–(60) using a Chebyshev collocation method (Trefethen 2000) to obtain a generalized algebraic eigenvalue problem, which is solved using the QZ algorithm in Matlab. Figure 3 shows the real part of the disturbance growth rate as a function of the cross-wind wavenumber k for various downwind wavenumbers l , with the uppermost curve in each plot corresponding to the $l = 0$ mode. For the given boundary conditions and Stokes drift profile, the first instability of the full 3D CL equations is found to occur at $La_c = (120)^{-1/2}$ for downwind-invariant modes (i.e. $l = 0$) with $k_c \rightarrow 0$. As shown in figure 3(a), the reduced dynamics exhibit an instability at finite k for La close to La_c , with the unstable modes taking the form of roll vortices aligned with the wind; close to the primary instability threshold, all 3D disturbances are damped. Under more strongly supercritical forcing conditions, however, there are exponentially growing 3D disturbances, as shown in figure 3(b). Nevertheless, the fastest-growing mode at $La = 0.01$ is strictly 2D. These results are in complete agreement with linear stability investigations of the full 3D CL equations (Leibovich and Tandon 1993).

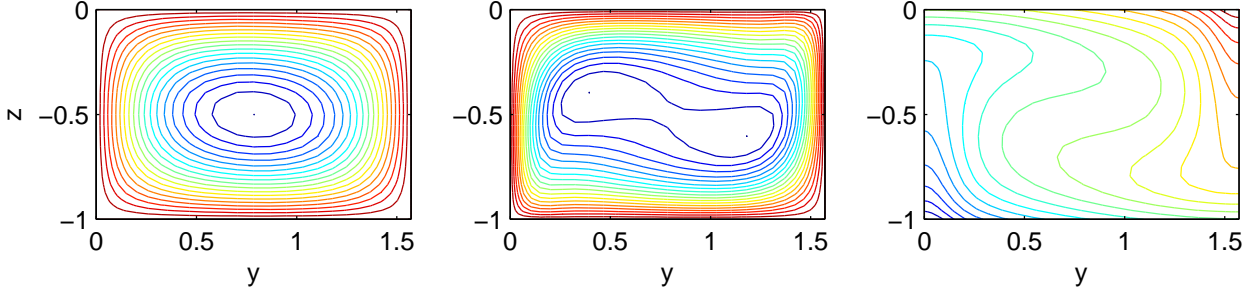


Figure 4. Steady, 2D finite-amplitude roll solutions of the CL equations at $La = 0.01$ computed numerically using a Fourier–Chebyshev pseudospectral method (with 30 Chebyshev modes and 64 Fourier modes). The fundamental cross-wind wavenumber of these solutions is $k = 2$; in each plot, only one cell is shown, since the solutions are reflection-symmetric. (a) Contours of $\psi(y, z)$ (left). (b) Contours of $\Omega(y, z)$ (middle). (c) Contours of $U(y, z)$ (right).

6.2 Secondary stability results

The linear stability analysis suggests that the reduced dynamics will be dominated by downwind-invariant disturbances, even for $La < La_c$. To investigate whether this prediction is borne out in the presence of nonlinearity, we have carried out a preliminary secondary stability analysis.

At $La = 0.01$, we numerically computed steady, 2D, fully nonlinear solutions to the CL equations using a Fourier–Chebyshev pseudospectral method, as described in Chini (2007). Figure 4 shows the structure of this nonlinear solution. We linearize the reduced equations about this finite-amplitude convective state by first expressing all fields as the sum of the cross-wind periodic, 2D nonlinear base flow (denoted with a subscript $2D$) and a time-varying 3D perturbation,

$$U(X, y, z, T) = U_{2D}(y, z) + u(X, y, z, T), \quad (61)$$

$$\psi(X, y, z, T) = \psi_{2D}(y, z) + \phi(X, y, z, T), \quad (62)$$

$$\Pi(X, y, z, T) = \Pi_{2D}(y, z) + p(X, y, z, T), \quad (63)$$

$$\Omega(X, y, z, T) = \Omega_{2D}(y, z) + \omega(X, y, z, T). \quad (64)$$

Note that $U_{2D}(y, z)$ includes the contribution from the wind-driven Couette flow $U_B(z)$. After substituting into (41)–(44) and (45)–(46), linearizing about the 2D cellular solution and eliminating $\omega(X, y, z, T)$, the equations and boundary conditions governing the evolution of the small-amplitude 3D disturbances can be expressed as

$$\partial_T u + \partial_z \psi_{2D} \partial_y u - \partial_y \psi_{2D} \partial_z u + \partial_y U_{2D} \partial_z \phi - \partial_z U_{2D} \partial_y \phi = -\partial_X p + La \nabla_{\perp}^2 u, \quad (65)$$

$$\begin{aligned} \partial_T (\nabla_{\perp}^2 \phi) + U_s(z) \partial_X (\nabla_{\perp}^2 \phi) + \partial_z \psi_{2D} \partial_y (\nabla_{\perp}^2 \phi) - \partial_y \psi_{2D} \partial_z (\nabla_{\perp}^2 \phi) \\ + \partial_y \Omega_{2D} \partial_z \phi - \partial_z \Omega_{2D} \partial_y \phi = U'_s(z) [\partial_y u - \partial_X (\partial_z \phi)] + La \nabla_{\perp}^4 \phi, \end{aligned} \quad (66)$$

$$\begin{aligned} \nabla_{\perp}^2 p = -4 \partial_y (\partial_z \psi_{2D}) \partial_y (\partial_z \phi) + 2 \partial_y^2 \psi_{2D} \partial_z^2 \phi + 2 \partial_z^2 \psi_{2D} \partial_y^2 \phi + U_s(z) \nabla_{\perp}^2 u \\ + U'_s(z) [\partial_z u + \partial_X (\partial_y \phi)], \end{aligned} \quad (67)$$

where, again, $U_s(z) = z + 1$, and along both $z = 0$ and $z = -1$,

$$\partial_z u = \phi = \partial_z^2 \phi = \partial_z p = 0. \quad (68)$$

Since the coefficients in (65)–(67) are independent of X and T and depend periodically on y , Floquet theory implies that solutions for the perturbation variables may be sought having the following form:

$$u(X, y, z, T) = e^{i\gamma y} \left[\sum_{n=-\infty}^{\infty} \hat{u}_n(z) e^{i(nky)} \right] e^{ilX} e^{\sigma t} + \text{c.c.}, \quad (69)$$

and analogously for $\phi(X, y, z, T)$ and $p(X, y, z, T)$. In (69), σ and l are the temporal growth rate and downwind wavenumber of the secondary instability mode; k is the fundamental wavenumber of the underlying 2D convective base flow; and the Floquet exponent is $i\gamma$, with the real parameter γ providing the freedom to modify the cross-wind wavenumber. Floquet representations of this sort were first introduced for secondary stability analyses in fluid dynamics by Kelly (1967) for inviscid shear flows, Clever and Busse (1974) for thermal convection, and Orszag and Patera (1983), Hebert (1983), Hebert (1988) and various other investigators for viscous shear flows. Tandon and Leibovich (1995) employed Floquet theory in their secondary stability investigation of LC using the full 3D CL equations. We follow Tandon and Leibovich (1995) by employing a Fourier–Chebyshev spectral method to discretize the differential eigenvalue problem, although we use a Chebyshev collocation method in the vertical coordinate rather than a tau method, as used by those authors. The resulting (large) generalized algebraic eigenvalue problem is again solved numerically using the QZ algorithm.

In figure 5, the real part of the growth rate of the dominant secondary instability mode is plotted as a function of the *downwind* wavenumber of the disturbance for two different base flow crosswind wavenumbers. In each plot, two curves are shown: the curve denoted by asterisks corresponds to the fundamental mode, with $\gamma = 0$, while the curve denoted by circles corresponds to the subharmonic mode, with $\gamma = k/2$. In the upper plot, the base flow wavenumber $k = 2$, corresponding to Langmuir cells having an aspect ratio around 1.5 (i.e. to slightly flattened cells), as is frequently observed in the upper ocean. Several features of this plot are noteworthy. First, although all downwind-invariant disturbances are either damped or neutrally stable, there are both fundamental and subharmonic 3D disturbances that grow exponentially on the convective time scale H/W_* . This result strongly suggests that the reduced system exhibits non-trivial nonlinear 3D dynamics, contrary to the conclusion drawn from the linear stability analysis of the base flow. Next, at least in this parameter regime, the fastest growing secondary instability is an oscillatory mode that propagates downwind with a phase speed equal to the depth-average value of $U_s(z)$ (i.e. $1/2$). This disturbance causes straight rolls to develop a waviness in the wind direction, as observed in field data (see e.g. figure 1(b)). Furthermore, the fundamental mode with the maximum growth rate has an $O(1)$ downwind wavenumber, suggesting that the rescaling of the downwind coordinate defined in § 4, *viz.* $X \equiv \varepsilon x$, is appropriate. These results agree with the findings of Tandon and Leibovich (1995), who observed that the downwind wavelength of the fastest-growing oscillatory mode increased as their parameter $R \equiv R_*^3 La_t^{-2}$ was increased with R_* held fixed; this limit is similar to the $\varepsilon \rightarrow 0$ limit investigated here. Finally, for $l \gg 1$, all 3D modes are damped, suggesting that the reduced system is not obviously ill-posed.

In the lower plot of figure 5, the base flow wavenumber $k = 2\pi$, corresponding to narrow cells. The secondary stability results for this case show that all 3D fundamental modes are damped, revealing a tendency for small-scale vortical structures to be strongly two-dimensionalized in the large CL vortex-force limit. A qualitatively similar behaviour has been noted by Poje and Lumley (1995) in their study of sheared Rayleigh–Bénard convection in the strong shear flow limit. Although there are unstable 3D subharmonic modes, the fastest-growing subharmonic mode occurs at $l = 0$. This sideband or Eckhaus instability, which was also found by Tandon and Leibovich (1995), indicates that a convective pattern in which the underlying 2D cells have a larger aspect ratio is preferred in this parameter regime.

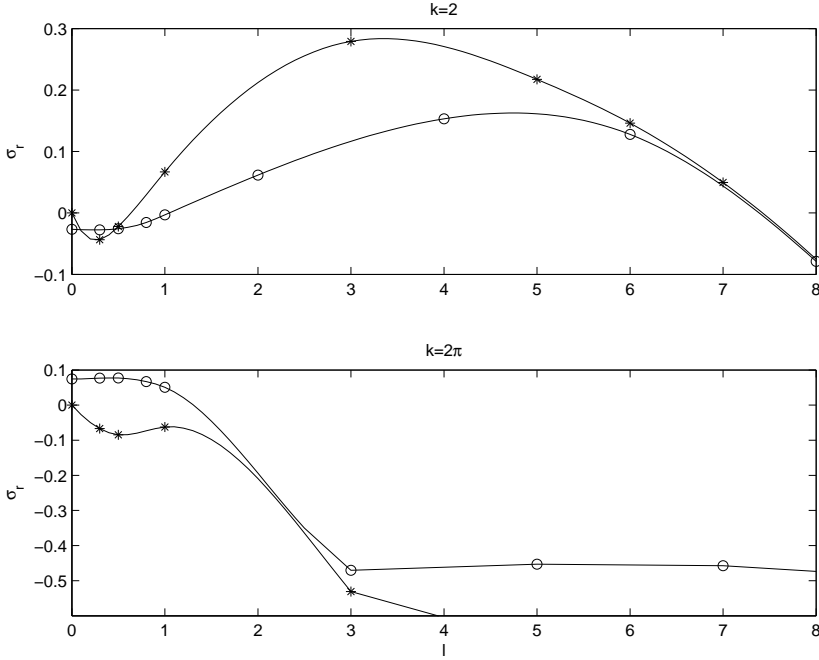


Figure 5. Secondary stability results for $La = 0.01$. The real part of the growth rate σ_r of the fastest-growing mode is plotted versus downwind wavenumber l for two different crosswind wavenumbers: (i) k (asterisks), the fundamental mode; and (ii) $k/2$ (circles), the subharmonic mode. (a) 2D base flow wavenumber $k = 2$ (upper). (b) 2D base flow wavenumber $k = 2\pi$ (lower). In all computations, the secondary instability modes were resolved with 30 Chebyshev modes in the vertical and up to 30 Fourier modes in the horizontal (cross-wind) direction.

7 Conclusion

Prior analytical, computational and observational studies all support the notion that Langmuir turbulence is anisotropic, being characterized by vortical structures elongated generally in the wind direction. Yet, previous theoretical and numerical investigations of strongly supercritical Langmuir circulation either have completely suppressed downwind variability, yielding a strictly 2D formulation, or have employed the full 3D CL equations. In the present work, we have sought an intermediate course by deriving a reduced model that appears to capture the essential physics of anisotropic Langmuir turbulence. The reduced equation set goes beyond the strictly 2D formulation by retaining downwind pressure gradients, advection of downwind vorticity by the surface-wave Stokes drift and the full contribution to the vertical vorticity in the CL vortex torque. Conversely, the reduced equations suppress certain aspects of the fully 3D dynamics, most notably advection by the downwind velocity component and stretching of the downwind vorticity, and can be cast in a streamfunction/scalar-vorticity form closely mimicking that frequently used for the strictly 2D problem.

Our reduced model of Langmuir turbulence is asymptotically exact in the limit that the turbulent Langmuir number $La_t \rightarrow 0$ with the friction Reynolds number R_* held fixed or allowed to grow at a rate less than La_t^{-2} . This flexibility in the range of allowed R_* is convenient: various investigators have asserted that $R_* = O(1)$, being based on an eddy viscosity arising from the CL wave-filtering procedure, while others maintain that $R_* \gg 1$ in actual geophysical applications. Notably, the results of several studies suggest that Langmuir turbulence seems to reach an equilibrated state that is relatively insensitive to R_* (however this parameter is interpreted) for $R_* \geq O(100)$ and oceanographically relevant values of La_t (see e.g. Tejada-Martinez and Grosch 2007). These results point to the importance of this latter parameter in controlling the nature of the strongly nonlinear dynamics: as $La_t \rightarrow 0$, as considered here, instabilities induced by the CL vortex force dominate shear-driven instabilities, and vortices aligned with the wind direction are preferred (as a cursory inspection of (1) reveals). We acknowledge that the actual numerical value of the parameter $\varepsilon \equiv R_*^{1/2} La_t$ used in our analysis may be close to unity in practice. Nevertheless, by formally treating ε as an asymptotically small parameter and employing the scalings adopted here, we perturb off a strictly 2D state and derive a physically sensible reduced model of strongly anisotropic

Langmuir turbulence.

Although we have not conducted a wide exploration of parameter space, the results of our linear and secondary stability analyses suggest that the reduced system should efficiently capture the dominant linear and secondary instabilities. Specifically, the linear stability predictions are, for 3D disturbances, in complete qualitative and, for 2D disturbances, quantitative agreement with linear stability analyses of the full 3D CL equations. (The latter assertion follows from the fact that when downwind variability is suppressed, our reduced set collapses exactly to the 2D CL equations.) Calculations based on both the reduced and full equations show that the first instability of the wind-driven unidirectional shear flow is to straight parallel (i.e. 2D) roll disturbances aligned with the wind. Above this primary instability threshold, growing 3D disturbances are found, but there exist 2D disturbances having larger growth rates. The results of preliminary secondary stability calculations reveal several intuitively-appealing features of our reduced model. 3D disturbances that grow exponentially on the convective time scale have been found in a parameter regime in which all 2D disturbances are damped; this strongly suggests that the reduced system exhibits non-trivial 3D dynamics. Moreover, the secondary instability mode with the maximum growth rate has an $O(1)$ downwind wavenumber, confirming the appropriateness of the rescaling (i.e. stretching by ε^{-1}) of the downwind coordinate employed in § 4 to capture slow streamwise variability. These findings also accord with the secondary stability results of Tandon and Leibovich (1995), who observed an apparent monotonic increase in the downwind wavelength of the fastest-growing secondary instability mode as their parameter $R \equiv R_*^3 La_t^{-2}$ was increased at fixed R_* . Furthermore, we note that the scalings employed in § 4 for the velocity components are qualitatively consistent with the results of LES by Tejada-Martinez and Grosch (2007). These authors showed that, for their “small” La_t sensitivity test ($La_t = 0.4$, $Re \equiv R_*/2 = 180$), the mean-square cellular velocity components (v and w) are much larger than the mean-square downwind velocity component (u). This finding is consistent with the assumed ratio of the downwind to cellular velocity scales $U_*/W_* = \varepsilon$.

The routine appearance of quasi-parallel windrows on the surface of wind-forced seas suggests that Langmuir turbulence is a commonly occurring upper ocean convective process. Indeed, there is ample evidence that Langmuir circulation is a key mixing mechanism in the ocean surface boundary layer. Although LES of the CL equations in limited domains have revealed important insights into the nature of Langmuir turbulence, one significant remaining challenge is to place this phenomenon in its larger oceanographic environment. It is hoped that asymptotically exact reduced formulations, of the sort derived here, may be used to facilitate, e.g., investigations of multiscale coupling between mixed layer turbulence and submesoscale and mesoscale eddies. Ultimately, improved parameterizations of the ocean mixed layer – schemes that are faithful to key underlying physical processes – are needed to better estimate air–sea interactions in ocean global general circulation models. In future work, we hope to adapt algorithms being developed for the efficient numerical simulation of strongly forced 2D Langmuir circulation to the reduced (quasi-3D) system derived here. We also plan to incorporate the combined effects of density stratification and Coriolis accelerations and to investigate other sets of scalings that may yield complementary reduced models of Langmuir turbulence valid in different parameter regimes. Finally, since streamwise vortex structures are a common feature of strongly unstable shear flows, we believe that our approach may be fruitfully applied to a wide range of shear-flow instability phenomena in geophysical and astrophysical settings.

GPC gratefully acknowledges funding for this work from NSF CAREER Award 0348981 administered by the Physical Oceanography Program.

REFERENCES

- Bhaskaran, R. and Leibovich, S. 2002. Eulerian and Lagrangian Langmuir circulation patterns. *Physics of Fluids* 14: 2557–2571
- Chini, G. P. 2007. Strongly nonlinear Langmuir circulation and Rayleigh–Bénard convection. *Submitted to the Journal of Fluid Mechanics*
- Chini, G. P. and Leibovich, S. 2003. Resonant Langmuir circulation–internal wave interaction. Part 1. Internal wave reflection. *J. Fluid Mech.* 495: 35–55
- Chini, G. P. and Leibovich, S. 2005. Resonant Langmuir circulation–internal wave interaction. Part 2. Langmuir circulation instability. *J. Fluid Mech.* 524: 99–120
- Clever, R. M. and Busse, F. H. 1974. Transition to time-dependent convection. *J. Fluid Mech.* 65: 625–645
- Cox, S. M. 1997. Onset of Langmuir circulation when shear flow and Stokes drift are not parallel. *Fluid Dynamics Research* 19: 149–167
- Cox, S. M. and Leibovich, S. 1994. Large-scale Langmuir circulation and double-diffusive convection: Evolution equations and flow transitions. *J. Fluid Mech.* 276: 189–210
- Cox, S. M. and Leibovich, S. 1997. Large-scale three-dimensional Langmuir circulation. *Phys. Fluids* 9: 2851–2863
- Cox, S. M., Leibovich, S., Moroz, I. and Tandon, A. 1992a. Hopf bifurcations in Langmuir circulations. *Physica D* 59: 226–254
- Cox, S. M., Leibovich, S., Moroz, I. and Tandon, A. 1992b. Nonlinear dynamics in Langmuir circulations with $O(2)$ symmetry. *J. Fluid Mech.* 669: 669–704
- Craik, A. D. D. 1977. The generation of Langmuir circulations by an instability mechanism. *J. Fluid Mech.* 81: 209–223
- Craik, A. D. D. and Leibovich, S. 1976. A rational model for Langmuir circulations. *J. Fluid Mech.* 73: 401–426
- Gnanadesikan, A. and Weller, R. 1995. Structure and instability of the Ekman spiral in the presence of surface gravity waves. *J. Phys. Oceanogr.* 25: 3148–3171
- Hebert, T. 1983. Secondary instability of plane channel flow to subharmonic three-dimensional disturbances. *Phys. Fluids* 26: 871–874
- Hebert, T. 1988. Secondary instability of boundary layers. *Ann. Rev. Fluid Mech.* 20: 487–526
- Julien, K., Knobloch, E., Milliff, R. and Werne, J. 2006. Generalized quasi-geostrophy for spatially anisotropic rotationally constrained flows. *J. Fluid Mech.* 555: 233–274
- Julien, K., Knobloch, E. and Werne, J. 1998. A new class of equations for rotationally-constrained flows. *Theoret. Comput. Fluid Dynamics* 11: 251–261
- Kelly, R. E. 1967. On the stability of an inviscid shear layer which is periodic in space and time. *J. Fluid Mech.* 27: 657–689
- Leibovich, S. 1977. On the evolution of the system of wind drift currents and Langmuir circulations in the ocean. Part 1. Theory and averaged current. *J. Fluid Mech.* 79: 715–743
- Leibovich, S. 1983. The form and dynamics of Langmuir circulations. *Ann. Rev. Fluid Mech.* 15: 391–427
- Leibovich, S. 1985. Oscillatory and competing instabilities in a nonlinear model for Langmuir circulations. *Phys. Fluids* 28: 2050–2061
- Leibovich, S., Lele, S. K. and Moroz, I. 1989. Nonlinear dynamics in Langmuir circulations and in thermosolutal convection. *J. Fluid Mech.* 198: 471–511
- Leibovich, S. and Tandon, A. 1993. Three-dimensional Langmuir circulation instability in a stratified layer. *J. Geophys. Res.* 98: 16,501–16,507
- Li, M. and Garrett, C. 1993. Cell merging and the jet/downwelling ratio in Langmuir circulation. *J. Mar. Res.* 51: 737–769
- Li, M. and Garrett, C. 1997. Mixed layer deepening due to Langmuir circulation. *J. Phys. Oceanogr.* 27: 121–132
- McWilliams, J. C., Sullivan, P. P. and Moeng, C. 1997. Langmuir turbulence in the ocean. *J. Fluid Mech.* 334: 1–30
- Orszag, S. A. and Patera, A. T. 1983. Secondary instability of wall-bounded shear flows. *J. Fluid Mech.*

128: 347–385

Pedlosky, J. 1987. *Geophysical Fluid Dynamics*. second edn, New York: Springer-Verlag

Poje, A. C. and Lumley, J. L. 1995. A model for large scale structures in turbulent shear flows. *J. Fluid Mech.* 285: 349–369

Skyllingstad, E. D. and Denbo, D. W. 1995. An ocean large-eddy simulation of Langmuir circulations and convection in the surface mixed layer. *J. Geophys. Res.* 100: 8501–8522

Sprague, M., Julien, K., Knobloch, E. and Werne, J. 2006. Numerical simulation of an asymptotically reduced system for rotationally constrained convection. *J. Fluid Mech.* 551: 141–174

Szeri, A. 1996. Langmuir circulations in Rodeo Lagoon. *Monthly Weather Review* 124: 341–342

Tandon, A. and Leibovich, S. 1995. Secondary instabilities in Langmuir circulations. *J. Phys. Oceanogr.* 25: 1206–1217

Tejada-Martinez, A. E. and Grosch, C. E. 2007. Langmuir turbulence in shallow water. Part 2. Large-eddy simulation. *J. Fluid Mech.* 576: 63–108

Thorpe, S. A. 2004. Langmuir Circulation. *Ann. Rev. Fluid Mech.* 36: 55–79

Trefethen, L. N. 2000. *Spectral Methods in Matlab*. Philadelphia: SIAM

List of Figure Captions

- (i) Figure 1. Images of Langmuir circulation windrows: (a) a photograph of Rodeo Lagoon in CA (Szeri 1996), (b) an infrared image of the surface of Tampa Bay (courtesy of G. Marmorino, NRL, D.C.), and (c) the evolution of surface tracers in a LES of Langmuir turbulence (McWilliams et al. 1997).
- (ii) Figure 2. Schematic of Langmuir circulation in a constant-depth unstratified layer. τ is the magnitude of the applied wind stress; u , v and w are the x -, y - and z -velocity components; and U_s is the depth-varying Stokes drift velocity associated with the filtered surface waves.
- (iii) Figure 3. Linear stability results. The real part of the growth rate σ_r of the fastest growing mode is plotted versus cross-wind wavenumber k for various downwind wavenumbers l . In each plot, $l = 0$ for the uppermost curve, and $l = 1, 2, 3, 4, 5, 6$ increasing downward. (a) $La = 0.08$ (left). (b) $La = 0.01$ (right). 30 Chebyshev modes were used for all computations.
- (iv) Figure 4. Steady, 2D finite-amplitude roll solutions of the CL equations at $La = 0.01$ computed numerically using a Fourier–Chebyshev pseudospectral method (with 30 Chebyshev modes and 64 Fourier modes). The fundamental cross-wind wavenumber of these solutions is $k = 2$; in each plot, only one cell is shown, since the solutions are reflection-symmetric. (a) Contours of $\psi(y, z)$ (left). (b) Contours of $\Omega(y, z)$ (middle). (c) Contours of $U(y, z)$ (right).
- (v) Figure 5. Secondary stability results for $La = 0.01$. The real part of the growth rate σ_r of the fastest-growing mode is plotted versus downwind wavenumber l for two different crosswind wavenumbers: (i) k (asterisks), the fundamental mode; and (ii) $k/2$ (circles), the subharmonic mode. (a) 2D base flow wavenumber $k = 2$ (upper). (b) 2D base flow wavenumber $k = 2\pi$ (lower). In all computations, the secondary instability modes were resolved with 30 Chebyshev modes in the vertical and up to 30 Fourier modes in the horizontal (cross-wind) direction.